Retrieval of Three-Dimensional Cloud Structure for Estimating Cloud-Radiative Forcing

L. Shi, J. del Corral, V. Ramanathan, and E. Boer
Scripps Institution of Oceanography
University of California at San Diego
La Jolla, CA 92039

The vertical structure of cloud-radiative heating plays an important role on the energy conversion and the dynamic structure of the atmosphere. To gain a better understanding of the three-dimensional cloud-radiative forcing field, Boer and Ramanathan (1992) have developed a three-dimensional imaging algorithm to reconstruct the three-dimensional structure of clouds from satellite advanced very high resolution radiometer (AVHRR) measurements. The algorithm combines a spatial coherence technique with spectral variations in reflectivities to identify clear-sky and adopts a delta-Eddington technique to retrieve cloud optical depths.

The algorithm is further refined in our current study. A discrete-ordinate radiative transfer model is used in this study to provide criteria for clear-sky detection and to obtain optical thickness from measured radiances. A prototype Atmospheric Radiation Measurement/Cloud and Radiation Testbed (ARM/CART) data set is employed to validate the cloud parameterization in the model. These data are provided by the Cloud Lidar And Radar Exploratory Test (CLARET) conducted in Boulder, Colorado, during September-October 1989 (Eberhard et al. 1992). The data set contains surface radiation measurements, atmospheric sounding, and cloud observations.

Comparison of Model Results with Surface Measurements

Three CLARET cases have been selected in our study: 1) stratus clouds on Day 276, 2) cirrus clouds on Day 271, and 3) mixed-phase clouds on Day 277. For the stratus cloud case, the depolarization signature of the ruby lidar showed only a water phase in the clouds. The cloud base altitude was between 700 and 950 meters above ground level. The cirrus clouds of Day 271 were situated within the altitude of 6-8 km. The microwave radiometer observed no detectable water, indicating that these clouds were composed mostly of ice. For the mixed cloud case on Day 277, visual observations revealed a variety of cloud types, including altocumulus, altocumulus undulatus, altostratus, cirrostratus, and wave clouds. The cloud base altitudes were at 3-5 km above ground level. The bulk structure of the clouds during the observation period was very complex, and the details changed considerably as the clouds advected over the site. Mixed liquid/ice water phase of clouds was detected.

Figure 1 shows the comparison of the model-calculated downward solar fluxes with the surface observations for Case 1. The data sets used by the model consist of vertical profiles of temperature and dew-point temperature, cloud base and penetration heights measured from a ruby lidar,

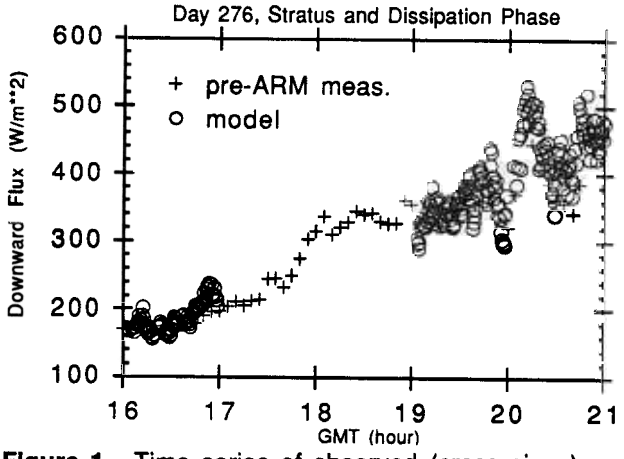

Figure 1. Time series of observed (cross signs) and modeled (circles) shortwave downward fluxes at the surface for Case 1 (stratus clouds).

and integrated liquid water path determined from a microwave radiometer. The cloud measurements have been averaged at every 30 seconds. In the figure, the circles represent the results calculated from the radiative transfer model; the cross signs represent the surface measurements (averaged at every 5 minutes) from a Pyranometer. The cloud effect in the model calculation is parameterized in terms of liquid water content and effective radius of the cloud drops, using the parameterization scheme developed by Ackerman and Stephens (1987). The values of effective radius are assumed to be 8 μm for the stratus cloud phase and 5 μm for the dissipation phase. The integrated liquid water path of the clouds during 16-17 GMT is 0.1-0.15 mm; the value decreases steadily to 0.01 mm during the dissipation phase of the clouds. Because of the absorption and reflection of the solar radiation by the stratus clouds, the downward shortwave flux reaching the surface is small (~200 $W \cdot m^{-2}$) in the stratus clouds phase, increasing to over 450 $W \cdot m^{-2}$ as the clouds thin out.

The general behavior of the modeled downward flux series is similar to that of the observational series, with smaller values in the stratus cloud phase and increasing values in the dissipation phase. Plane-parallel assumption has been used in the model calculation. The general agreement between the model results and measurements indicates that the plane-parallel assumption can simulate the stratiform cloud condition well.

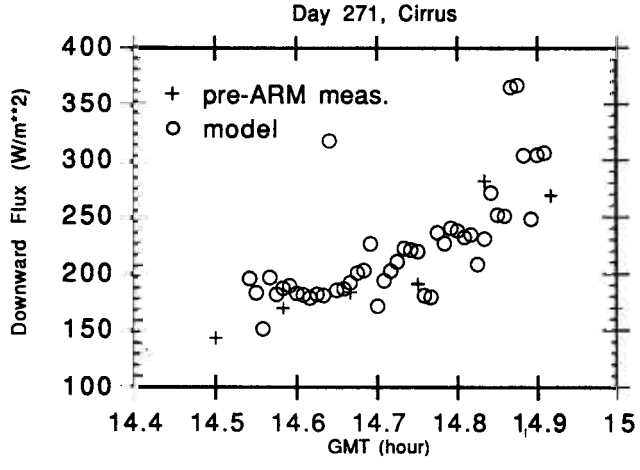

Figure 2. Time series of observed (cross signs) and modeled (circles) shortwave downward fluxes at the surface for Case 2 (cirrus clouds).

The intercomparison for Case 2 is shown in Figure 2. The cirrus parameterization scheme from the study of Takano and Liou (1989) has been used in the model calculation. In their study, the extinction coefficient, single scattering albedo and asymmetry factor in the shortwave spectrum were computed based on the observed ice crystal size distributions for four typical cirrus clouds, i.e., cirrostratus, cirrus uncinus, warm cirrus, and cold cirrus. The optical properties of warm cirrus and cirrus uncinus have been used in our model calculations for the clouds with thickness larger than 1 km and less than 1 km, respectively. There is a 7-hour difference between the Greenwich Mean Time (GMT) and the local solar time (LST) of the site. Thus, the local solar time corresponding to the GMT shown in Figure 2 is 7.5-8 LST. The solar flux increasing with time is partly due to the increasing solar radiation and partly due to the thinning clouds.

In Figure 2, three modeled results have much higher values than the observations; one is found between 14.6 and 14.7 GMT and the other two are found between 14.8 and 14.9 GMT. For these three points, the CLARET data set reports no clouds detected by the radar. Thus clear-sky condition has been used in the model calculation. We suspect that very thin clouds were present at the time; however, the signal was too weak to be detected by the radar.

For the mixed-phase cloud (Case 3) depicted in Figure 3, the intercomparison shows more deviation of the model

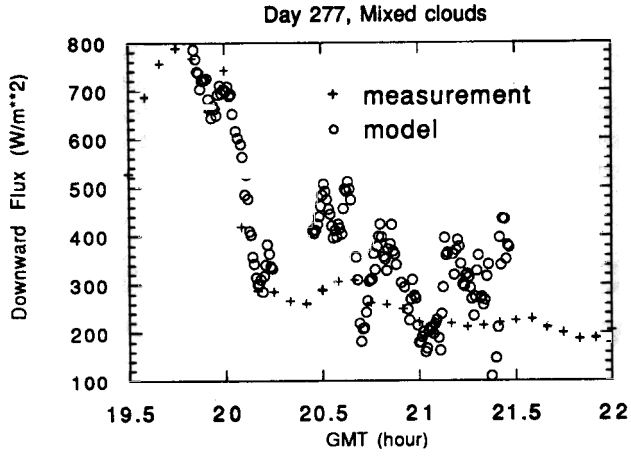

Figure 3. Time series of observed (cross signs) and modeled (circles) shortwave downward fluxes at the surface for Case 3 (mixed-phased clouds).

results from the surface measurements. At the beginning of the cloud series when both liquid and ice water paths of the clouds are small, the model results agree well with the surface observation. However, as more clouds move into the region, the differences increase.

These differences result from a combination of factors. First, plane-parallel assumption is used in the model calculation. This assumption might not work as well as for stratiform clouds; some of the deviation might be caused by cloud side effects. Second, the cloud-microphysics changes considerably with time. However, a constant value of 5 μm is assumed for the effective radius of clouds in the model calculation. Third, the surface radiation measurement represents the integrated cloud effects from the whole sky; whereas, the lidar measures the clouds only at the zenith. This explains the much larger variation among cloud measurements than among surface radiation measurements.

Improvement of the 3-D Cloud Retrieval Algorithm

Coakley and Bretherton (1982) have developed a technique for determining clear and cloudy sky radiances using the spatial coherence method. The method uses the local spatial structure of the radiance field to determine the radiances associated with cloud-free and completely cloud-covered fields of view. This approach is used in the present study as the first criterion for detecting a clear-sky pixel.

The second criterion for determining a clear-sky pixel is based on threshold values calculated by the discrete-ordinate radiative transfer model. We have found that the clear-sky reflectivities of channels 1 and 2 can vary significantly, not only with respect to the solar zenith angle but also with respect to the satellite zenith angle. With this consideration, the threshold values for upper-bond of clear-sky reflectivities are calculated at the full satellite span angle as a function of solar zenith angle.

Color information from the visible channels is employed in setting the third criterion for clear sky detection. As the spectral band widths of channels 1 and 2 are approximately 0.58-0.68 μm and 0.725-1.10 μm, respectively, the reflectivity value of the shorter wavelength channel (channel 1) should be higher than that of the longer wavelength channel (channel 2) for a clear-sky pixel; and the reflectivity values of the two channels should be very close to each other if the pixel is completely filled with a thick cloud. A pixel is considered to be cloudy if the reflectivity ratio of channel 1 to channel 2 is smaller than the threshold value at the corresponding solar zenith angle.

The pixels which fail to meet one or more of the clear-sky criteria are classified as cloudy pixels. Cloud-top altitude of each pixel is calculated according to cloud-top temperature. Cloud optical thickness (t) is obtained by comparing the observed pixel reflectivity value in channel 1 to the reflectivity value calculated from the radiative transfer model. Because a cloudy pixel can have different reflectivity values when it is observed at different satellite zenith angles, the reflectivities with respect to different zenith angles have been calculated by the model. The cloud-base altitude is derived from cloud optical thickness and extinction coefficient. A visualization algorithm is applied to display the 3-D clouds for verifying visually the cloud reconstruction scheme. Further work will be done to improve the cloud reconstruction scheme by collocating the satellite and surface measurements of clouds from the Southern Great Plains site in Oklahoma.

Future Work

The satellite and surface measurements of clouds and radiation fields from the ARM Western Pacific site will be used in our study to estimate the three-dimensional structure of the atmospheric cloud-radiative forcing. The estimation will help to understand the relationship between the large-scale moisture and radiative heating fields. The analyses will also provide a basis to examine the parameterizability of clouds in general circulation model studies and to investigate the role of cloud-radiative feedbacks on the sea surface temperature.

References

Ackerman, S. A., and G. L. Stephens. 1987. The absorption of solar radiation by cloud droplets: An application of anomalous diffraction theory. J. Atmos. Sci. **44**:1574-1588.

Boer, E., and V. Ramanathan. 1992. Three dimensional imaging of cloud structure using satellite radiances: A new tool for cloud studies. 1992 AGU Spring Meeting (abstract).

Coakley, J. A., Jr., and F. P. Bretherton. 1982. Cloud cover from high-resolution scanner data: Detecting and allowing for partially filled fields of view. J. Geophy. Res. **87**:4917-4932.

Eberhard, W. L., T. Uttal, K. A. Clark, R. E. Cupp, E. G. Dutton, L. S. Fedor, J. M. Intrieri, S. Y. Matrosov, J. B. Snider, and R. J. Willis. 1992. Remote sensing data from CLARET: A prototype CART data set. NOAA Technical Memorandum ERL WPL-223,1-58.

Takano, Y., and K.-N. Liou. 1989. Solar radiative transfer in cirrus clouds. Part 1: Single-scattering and optical properties of hexagonal ice crystals. J. Atmos. Sci. **46**:3-19.